Alpha particle spectroscopy using FNTD and SIM super-resolution microscopy

Kouwenberg, J. J.M.; Kremers, G. J.; Slotman, J. A.; Wolterbeek, H. T.; Houtsmuller, A. B.; Denkova, A. G.; Bos, A. J.J.

DOI
10.1111/jmi.12686

Publication date
2018

Document Version
Final published version

Published in
Journal of Microscopy

Journal of Microscopy

Journal of Microscopy, Vol. 270, Issue 3 2018, pp. 326–334 doi: 10.1111/jmi.12686
Received 11 September 2017; accepted 12 January 2018

Alpha particle spectroscopy using FNTD and SIM super-resolution microscopy

J.J.M. KOUWENBERG*, G.J. KREMERS†, J.A. SLOTMAN†, H.T. WOLTERBEEK*, A.B. HOUTSMULLER†, A.G. DENKOVA* & A.J.J. BOS*

**Radiation, Science & Technology, Technische Universiteit Delft Faculteit Technische Natuurwetenschappen, Mekelweg 15, Delft, the Netherlands*

†Erasmus Optical Imaging Centre, Erasmus MC, 's-Gravendijkwal 230, Rotterdam, the Netherlands

Key words. Alpha radiation, FNTD, SIM.

Summary

Structured illumination microscopy (SIM) for the imaging of alpha particle tracks in fluorescent nuclear track detectors (FNTD) was evaluated and compared to confocal laser scanning microscopy (CLSM). FNTDs were irradiated with an external alpha source and imaged using both methodologies. SIM imaging resulted in improved resolution, without increase in scan time. Alpha particle energy estimation based on the track length, direction and intensity produced results in good agreement with the expected alpha particle energy distribution. A pronounced difference was seen in the spatial scattering of alpha particles in the detectors, where SIM showed an almost 50% reduction compared to CLSM. The improved resolution of SIM allows for more detailed studies of the tracks induced by ionising particles. The combination of SIM and FNTDs for alpha radiation paves the way for affordable and fast alpha spectroscopy and dosimetry.

Introduction

The use of alpha particle emitting radionuclides for the treatment of cancer is increasing rapidly (Sofou *et al.*, 2004; Sartor *et al.*, 2012; Jadvar & Quinn, 2013; Bandekar *et al.*, 2014). Alpha radiation has a high Lineal Energy Transfer (LET), a measure for the amount of energy deposited per distance travelled, which leads to high biological effectiveness (Franken *et al.*, 2011; Tracy *et al.*, 2015) and insensitivity to the oxygen concentration in the tumour (Barendsen *et al.*, 1966; Sgouros *et al.*, 2010). This can be a promising prospect for the treatment of tumours resistant to conventional radiation therapy (Elgqvist *et al.*, 2014). Unfortunately, to this day alpha radiation spectroscopy and dosimetry remain challenging due to the short range of alpha particles (less than 100 μm in water) (Sgouros *et al.*, 2010). Improvements in such measurements are expected to greatly enhance the development of alpha particle mediated cancer treatment.

Fluorescent nuclear track detectors (FNTD) have shown to be an excellent tool for alpha radiation research (Sykora *et al.*, 2009; Kouwenberg *et al.*, 2016), offering a high spatial resolution in combination with fast and stable read-out using confocal laser scanning microscopy (CLSM). FNTDs are aluminium oxide crystals with carbon and magnesium dopants, giving them a characteristic green colour (M. S. Akselrod *et al.*, 2006). The dopants introduce defects in the crystal, called colour centres, that undergo radiochromic transformations when irradiated (G. M. Akselrod *et al.*, 2006). These transformed colour centres are very stable and are fluorescent with an excitation wavelength of ~650 nm and emission at 750 nm. The FNTD can therefore be imaged using fluorescence microscopy to yield high-resolution images of the tracks induced by passing alpha particles in the crystal (Bartz *et al.*, 2013). The direction, length and spatial scattering of these tracks is used to calculate the initial energies and directions of alpha particles. From this the various characteristics of the alpha radiation field, like absorbed dose rate and biological effectiveness, can be deduced. The spatial and energy resolutions of alpha tracks in FNTDs are however restricted by the resolution limit of CLSM. Here, we investigated the use of an alternative fluorescence super-resolution microscopy technique, structured illumination microscopy (SIM) (Lukosz & Marchand, 1963; Gustafsson *et al.*, 2008), for FNTD read-out, utilising both its fast read-out and high spatial resolution to improve spatial and energy resolution in alpha radiation measurement.

Materials and methods

FNTD Irradiation

Al_2O_3:C,Mg Fluorescent Nuclear Track Detectors (Landauer, Inc., Glenwood, Illinois, USA), kindly donated by Landauer, Inc., were irradiated using a 1.1 cm diameter 394 kBq

J.J.M. Kouwenberg and G.J. Kremers contributed equally to the work.

Correspondence to: Jasper J M Kouwenberg, Radiation, Science & Technology, Delft University of Technology, Mekelweg 15, Delft, the Netherlands. Tel: +31 15 27 87053; e-mail: j.j.m.kouwenberg@tudelft.nl

Am-241 source with an estimated 1.3 μm layer of americium oxide and a 2 μm protective gold layer (Czech Metrological Institute, Brno, Czech Republic), placed behind a 3D printed honeycomb collimator. The honeycomb collimator restricted outgoing alpha particles to a maximum vertical angle of ~45°, a requirement for sufficient penetration in the FNTD (Kouwenberg *et al.*, 2016). Four $8 \times 4 \times 0.5\,mm^3$ FNTDs were irradiated at a $5.00 \pm .05$ mm distance from the source for 267 s each above the centre of the collimator to induce an approximate water equivalent dose of 1 Gy in the detector.

FNTD Read-out

Small arbitrarily chosen volumes near the centre of the FNTDs were read-out using both CLSM and SIM super-resolution microscopy. The measured volumes were not the same for both devices. A Leica SP5 (Leica Microsystems, Mannheim, Germany) with an Avalanche Photo Diode (APD) behind a Chroma Technology ET655lp 655 nm long pass filter (Chroma Technology Corp., Bellows Falls, Vermont, USA) together with a 633 nm excitation laser was used in the CLSM read-out. A HCX PL APO CS 63 × 1.4 NA Oil objective, 2.5 zoom factor, 40 Hz scan speed and 2 times line averaging were used to yield 96 × 96 × 490 nm^3 sized voxels in a 98 × 98 × 10 μm^3 read-out volume. Imaging of one read-out volume took 25 min and no post-processing was performed on the resulting images.

SIM imaging was performed on a Zeiss Elyra PS1 with an Andor iXon DU 885 EMCCD camera (Carl Zeiss AG, Oberkochen, Germany) behind a LP655 filter with a Plan Apochromat DIC 63 × 1.4 NA Oil objective and 642 nm laser excitation with 500 ms exposure times and EM gain set at 30. Samples were illuminated with a spatial line pattern that was shifted in five phases and rotated in five orientations. The raw images were reconstructed (Gustafsson *et al.*, 2008) into a high-resolution 3D-dataset using the Zeiss 2012 PS1 ZEN software. Reconstruction was done using default settings. Sectioning values for filtering of zero, first and second order peaks in the Fourier transformed images were 100, 83 and 83 respectively, where 100 is maximum filtering and 0 is no filtering. Noise filtering was done using a generalised Wiener filter with a regularisation parameter of 10^{-6}. No correction was made for anisotropy and the results were baseline shifted. The SIM check toolbox (Ball *et al.*, 2015) was used to evaluate the SIM reconstruction results. SIM reconstruction yielded 39.7 × 39.7 × 144 nm^3 sized voxels in a 75 × 75 × 10 μm^3 read-out volume. Imaging of one read-out volume took 18 min.

Signal-to-noise ratios (SNR) were calculated via:

$$SNR\ (\pm\sigma) = \frac{\mu_t\,(\pm\sigma_t) - \mu_b}{\sigma_b}, \qquad (1)$$

where μ_t and σ_t are respectively the mean and standard deviation of the measured track intensities, whereas μ_b and σ_b are respectively given by the mean and standard deviation of the background intensity.

Table 1. Feature point linking parameters for CLSM and SIM.

Parameter	CLSM	SIM	Parameter	CLSM	SIM
$\boldsymbol{I}$	3 a.u.	5500 a.u.	$\boldsymbol{w_d}$	0.5	0.5
$\boldsymbol{r} = \boldsymbol{r_p}$	6 px	6 px	$\boldsymbol{w_i}$	1	0.2
$\boldsymbol{d_{p,\max}}$	10 px	20 px	$\boldsymbol{w_v}$	0.5	1
$\boldsymbol{R}$	3	3	$\boldsymbol{w_a}$	1	1
$\boldsymbol{\theta_{p,\max}}$	30°	30°	$\boldsymbol{d_{t,\max}}$	30 px	40 px
$\boldsymbol{H}$	4	4	$\boldsymbol{D_{\max}}$	$10 \cdot C_{\max}$	$10 \cdot C_{\max}$

Resolution measurement

A line was fitted through the maximum Z projection of all tracks in a field of view in FIJI (Schindelin *et al.*, 2015). A Gaussian model was fitted to the average intensity profile perpendicular to the track at a single pixel spacing, using the nonlinear least squares algorithm in the software package R version 3.2.2 (R Core Development Team, 2011). Track diameter was defined as the FWHM (full width half maximum) calculated via:

$$FWHM = 2\sqrt{2\ln 2}\,\sigma, \qquad (2)$$

where σ is the fitted standard deviation.

Particle tracking

The fluorescent tracks produced by the alpha particles in the FNTDs consist of series of fluorescent spots in the 2D images. Track reconstruction is required for further analysis of the tracks. The fluorescent spots were used for track reconstruction using an expanded version of in-house built software. Spots in the 2D images were connected to reconstruct the tracks based on proximity and similarity in trajectory and intensity. This procedure is described in more detail in a previous publication (Kouwenberg *et al.*, 2016). A summary of the tracking parameters used in said publication for the CLSM and SIM sets are given in Table 1. I is the intensity threshold for spot selection, r and r_p are related to the spot size and drift, $d_{p,\max}$ and $d_{t,\max}$ are related to the maximum distance between spots for linking, R and H control the minimum number of spots per track and the amount of spots used for track averaging, $\theta_{p,\max}$ is the maximum allowed angle and w_d, w_i, w_v and w_a are the weighting factors for respectively distance, intensity, velocity and angle. $D_{\max}$ is the maximum allowed cost for track relinking.

Range estimation

Let l be a set of trajectories in image stack A, where each trajectory contains a set of N points p_i (Fig. 1). Each point can be described using its coordinates x_i, y_i, z_i, given in voxels from the image stack origin, and intensity I_i. The intensity was taken as the average of the five centre voxels of a spot whereas

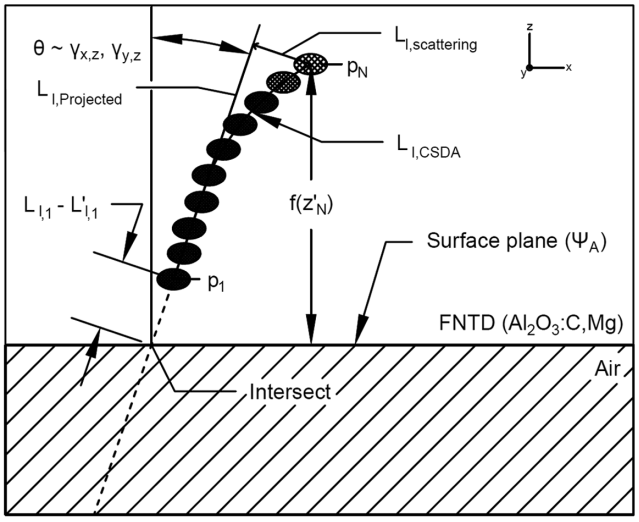

Fig. 1. Schematic of an alpha particle penetrating a FNTD, producing a series of fluorescent spots (p_1 .. p_n) in the CLSM and SIM images. The depth in the FNTD of a spot p_i is given by $f(z'_i)$, and the separation between spots in the z-direction is determined by the respective step-size of the measurement. The initial trajectory of the particle upon entering the FNTD ($\gamma_{x,z}, \gamma_{y,z}$) is determined using the first five spots of the track. The distance travelled through the FNTD by the alpha particle before the first spot is measured, is determined using this trajectory and the surface plane of the FNTD. The lateral scattering ($L_{l,scattering}$) is given by the perpendicular deviation from the initial trajectory of the track, measured at the last fluorescent spot within the track. Fluorescence intensity decay at the end of a track is illustrated by the change in the brightness of the spots.

the x and y coordinates followed from intensity weighting of the same voxels. Each coordinate is given as the far corner of a voxel, that is the first voxel is given by (1, 1, 1). Reflectance imaging was used to establish the angle of the surface plane. In cases where the location of the surface plane was later located using the lengths of the measured tracks, 25% of the measured tracks were used for surface plane localisation, whereas the remaining 75% of the tracks were used for spectroscopy purposes (see Results and Discussion). Let the surface plane of image stack A obtained from the maximum reflectance be given by $\Psi_A(x, y, z) \equiv \psi_x x + \psi_y y - z = -z_0$, so that the corrected z-coordinate is given by

$$z'_i = z_i - \psi_x x_i - \psi_y x_i - z_0. \tag{3}$$

The length $L'_{l,i}$ of track l at point i is then given by

$$L'_{l,i} = \sum_{j=1}^{i-1} \sqrt{s_x^2 (x_{j+1} - x_j)^2 + s_y^2 (x_{j+1} - x_j)^2 + \left(f\left(z'_{j+1}\right) - f\left(z'_j\right)\right)^2}, \tag{4}$$

where s_x, s_y are the voxel sizes in μm in the x and y direction as given by the microscopy control software. f is a function for the depth correction required for the refractive index mismatch between the immersion oil ($n = 1.518$) of the objective and Al_2O_3 ($n = 1.765$), given by Eq. (13) in Van Elburg *et al.* (Van Elburg *et al.*, 2007). The total penetration of track l follows from the length of the track and the intersection of the initial track direction with Ψ_A. Because the slope of the surface plane is often small compared to the slope of the tracks, the distance between p_1 and the point of intersect can be simplified to:

$$L_{l,i} = L'_{l,i} + \frac{f\left(z'_1\right)}{\sqrt{1 + \chi_l^2 + \gamma_l^2}}, \tag{5}$$

where χ_l is the linear slope between $s_x x_i$ and $s_z(z'_1) \cdot z'_1$, and γ_l is the linear slope between $s_y y_i$ and $s_z(z'_1) \cdot z'_1$, both based on the first five points.

The position of the end of the track was refined using the fluorescence intensity I. Because the colour centre concentration in the FNTDs is low (G. M. Akselrod *et al.*, 2006), colour centre saturation inside the track is expected to occur at a Linear Energy Transfer (LET) far below the average LET of an alpha track. For samples with a good SNR, an exponential function was fitted to the fluorescence intensity I_i as function of track length $L_{l,i}$ in accordance with the dose profile of the alpha track (Cucinotta *et al.*, 1998):

$$I_{fit}(L_{l,i}) = a + (1 - a)(1 - e^{-b \cdot (L_{l,i} - L_{l,N})}), \tag{6}$$

where the parameters a and b were fitted using the implementation of the Broyden–Fletcher–Goldfarb–Shanno algorithm as found in software package R version 3.2.2. The endpoint of the track was chosen at $I_{fit} = 95\,\%$ because it is theorised that colour centre saturation happens at LETs far below those of alpha particles. The drop in intensity therefore indicates the end of the alpha particle track. Residual energy deposition is the result of high-energy delta rays travelling beyond the path of the alpha particle (Scholz & Kraft, 1996). The fitting was limited to 2.5 μm from the endpoint to avoid faulty fitting due to scattering of the alpha particle within the track. For cases where the SNR was too low for accurate fitting, the endpoint was chosen, when possible, as the last point with an intensity above the mean track intensity minus the track intensity standard deviation. When either method failed, no further refinement was attempted.

The detour factor is an indicator for the deviation of the track from a straight line of a particle in a material and is defined as:

$$Detour\ factor \equiv \frac{L_{l,\ projected}}{L_{l,\ CSDA}}, \tag{7}$$

where $L_{l,\ projected}$ is the track length projected onto the initial track direction vector and $L_{l,\ CSDA}$ is the Continuous Slowing Down Approach (CSDA) range which is given here by the procedural track length as described by Eq. (5). The scattering is defined here as the deviation from the projected orthogonal

to the projection vector ($L_{l,scattering}$). The relative scattering can then be expressed as

$$Relative\ scattering \equiv \frac{L_{l,scattering}}{L_{l,CSDA}}. \quad (8)$$

The code framework for track following and calculation was written in a combination of the software packages R version 3.2.2 and Java version 8.

Energy calculation

Alpha particles originate in a 1.3 μm thick Am_2O_3 layer and pass through a 2 μm layer of gold and then a 5 mm air layer before entering the FNTD. Using the approximated initial direction vector $z = \chi_l\, x + \gamma_l\, y$, the path length through the kth layer, denoted as $\tau_l^{(k)}$, could be estimated using the equation below, assuming that the track passes through the whole layer.

$$\tau_l^{(k)} = \frac{t^k}{\sqrt{1 + \chi_l^2 + \gamma_l^2}}, \quad (9)$$

where t^k is the thickness of the kth layer. This approach ignores scattering in either layer. The path length of an alpha particle can be related to its loss of energy using translation tables, which in this case were obtained from the ASTAR application by the National Institute of Standards and Technology, USA (NIST) (Berger *et al.*, 2005). The energy loss of an alpha particle passing through a layer is then given by

$$\Delta e_l^{(k)} = e_l^{(k-1)} - e_{mat}\left[R_{mat}\left(e_{l,0}^{(k-1)}\right) - \tau_l^{(k)}\right], \quad (10)$$

where e_{mat} is a conversion function for the residual range to the corresponding energy in a material and R_{mat} acts as the inverse of e_{mat} and $e_l^{(k-1)}$ is the particle's energy the moment it leaves layer $k-1$ and enters the kth layer. The total energy of an alpha particle then follows from iteration of Eq. (10) for each layer including the FNTD, where $\tau_l^{(FNTD)}$ was given by the refined track length. When the depth z_0 of the surface plane could not be found, it could be retrieved by optimisation of z_0 for $|e_{peak} - e_{Am241}| \approx 0$, where e_{peak} is the peak in the measured energy distribution for image stack A and e_{Am241} is the mean alpha energy for Am-241.

FLUKA simulation

A simulation was built in FLUKA 2011.2c.5 (Ferrari *et al.*, 2011) to measure the energy distribution of alpha particles entering the FNTD. The collimator was modelled as the material BLACKHOLE to improve calculation speed. The source was modelled as an infinitely thin layer halfway within the americium oxide layer, which was modelled using the same density, but with gold atoms to approximate americium atoms because higher Z atoms are not available in FLUKA. The energies of 10^7 incoming alpha particles were measured with the FLUKA function USRBDX in 30 keV bins.

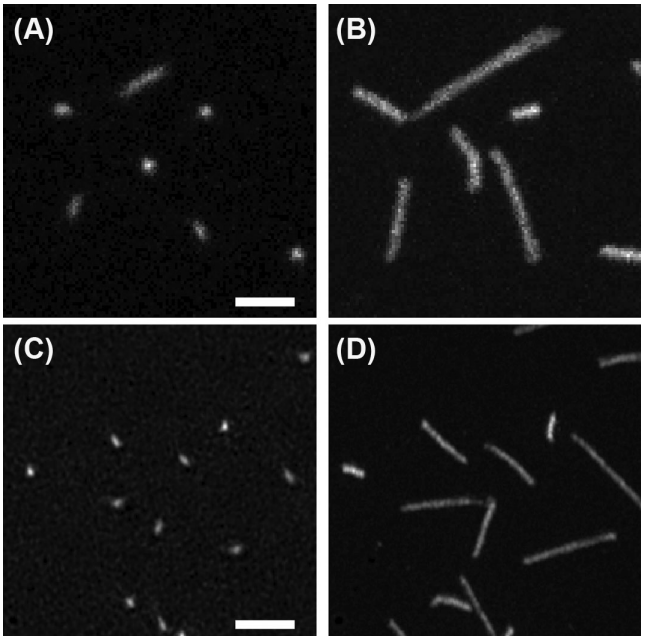

Fig. 2. Close-up of FNTDs irradiated with alpha radiation and imaged with CLSM (A and B) and SIM (C and D). Panels A and C show single images and panels B and D show the maximum projection of the 3D image stacks. Scale bars are 2 μm. Note that panels A and B show a different field of view than panels C and D.

Results and discussion

To compare SIM and CLSM imaging for FNTD-based alpha particle spectroscopy, four randomly chosen areas were scanned using both modalities. Because the range of an alpha particle in matter is directly related to its energy, the surface plane for both the SIM and CLSM scans were found by matching the calculated pathlength of alpha particle tracks through the FNTD, together with the observed angle of incidence and known pathlength through the air and source, to the energy of alpha particles emitted by the source. Am-214 emits alpha particles with 2 possible energies: 5486 keV (85% chance) and 5443 keV (15% chance). The energy difference of 43 keV would not be expected to be distinguished due to the thickness of the test material and variations in angle of incidence that would degrade the fidelity of the energies impinging on the FNTD. Indeed, even conventional alpha spectrometers can be challenged by this energy separation for thick specimens. An average alpha particle energy of 5480 keV was therefore assumed.

Figure 2 shows a close-up of an area imaged with CLSM and SIM, respectively. The full field of view of the scans is shown in Fig. S1.

In single optical sections nuclear fluorescent tracks appeared as round or elongated spots (Figs. 2A, C and S1A). Round spots referred to alpha particles, which propagated nominally perpendicular to the FNTD surface (i.e. the imaging plane). Spot elongation was caused by a combination of the incident angle of the alpha particle trajectory with the FNTD and the optical slice thickness of the microscope. Shallow angle tracks were identified by more elongated spots in single sections and their apparent increase in length in a maximum projection along the *z* axis (Figs. 2B, D and S1B, D). Spot elongation was less for SIM, as a result of the improved optical sectioning capability. SIM imaging yielded a SNR (14.4 ± 4.8) comparable to CLSM (13.9 ± 3.6).

The radial track profile was predicted to be in the order of 3 to 100 nm (Cucinotta *et al.*, 1998). Here, we measured the radial track profile as the FWHM perpendicular to the length of the alpha tracks. As expected, the SIM images showed smaller track diameters (FWHM 209 ± 69 nm), compared to CLSM (FWHM 322 ± 19 nm). The fact that these values are somewhat higher than the theoretical resolution limits for SIM (140 nm) and CLSM (280 nm; pinhole 1 airy unit) might be explained by the large difference in wavelength between excitation (647 nm) and emission (750 nm). In addition, the anisotropic properties of the FNTD material (see below) could have negatively affected the measured track width. However, it is noteworthy that the radial track profile found in FNTDs irradiated with 3 MeV protons (LET in Al_2O_3: 35 keV μm^{-1}) and 1094 MeV carbon ions (LET in Al_2O_3: 90 keV μm^{-1}), imaged by stimulated emission depletion (STED) microscopy, yielded comparable track diameters of respectively 196 ± 28 nm and 240 ± 29 nm (FWHM) (Niklas *et al.*, 2017). Note that, 3.7 MeV alpha particles, used for this work, have a LET in Al_2O_3 of 308 keV μm^{-1} (Berger *et al.*, 2005).

For SIM imaging the orientation of the FNTD on the microscope was important, due to the optically anisotropic properties of Al_2O_3:C,Mg (Akselrod *et al.*, 2003). The FNTDs were cut with the 'c' optical axis along the long axis of the chip (Akselrod, personal communication). Hence the 'c' optical axis was perpendicular to the optical axis of the microscope and more than one refractive index could be observed in the imaging plane. We expected that polarisation dependent fluctuations in the fluorescence yield might adversely affect SIM image reconstruction. To test this, FNTDs were imaged at different orientations. Shadow images were observed next to the fluorescent tracks, but appeared to be absent when FNTDs were oriented at 0° (Fig. S2). The expected variation in the separation distance between the shadow images and the main fluorescent track should be dependent on the track's angle of incidence relative to the detector surface and therefore the thickness of the FNTD through which the imaging is performed. These observations still need to be compared to the theoretical separation based on track depth and crystallographic orientation of the FNTD. Nevertheless, all subsequent SIM measurements were done under conditions that eliminated the observation. In addition, we used the SIMcheck toolbox (Ball *et al.*, 2015) to identify putative problems with the 3D-SIM reconstructions. This analysis verified that the raw and processed SIM data were of good quality and showed no evidence for common SIM reconstruction issues (Fig. S3).

Because of the increased resolution of SIM compared to CLSM, we expected SIM imaging of FNTDs to allow for more detailed studies of the tracks induced by ionising particles. Plotting the normalised fluorescence intensity as function of distance from the track resulted in the intensity profiles shown in Figure 3. Note that the visible gaps are the result of the discrete step-size in *z*-direction. An exponential intensity decay

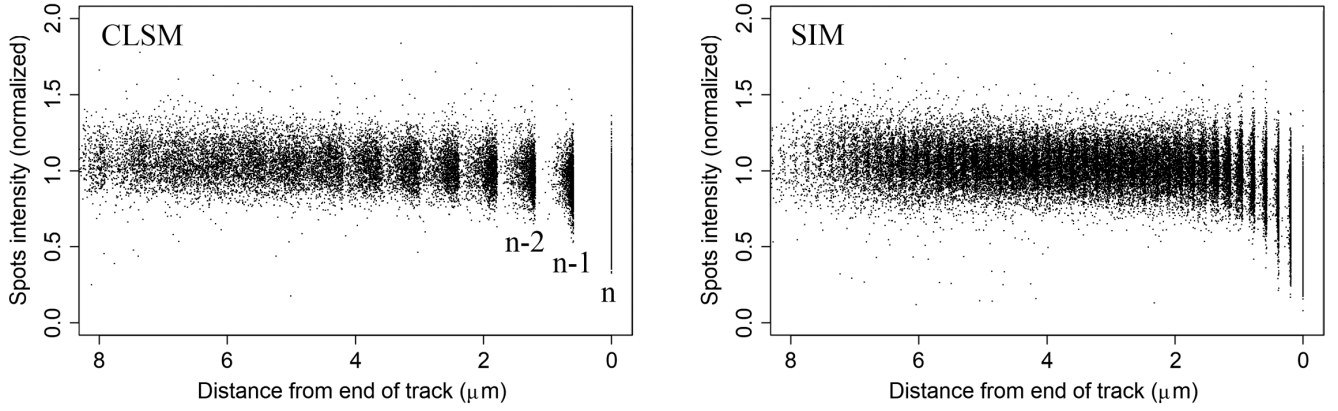

Fig. 3. Scatter plot of the normalised fluorescence intensity of spots as function of distance from the last detected spot (indicated by *n*) in their respective track. An exponential decay of fluorescence is visible for CLSM (left) and SIM (right). Note that the distance between two spots for a track perfectly perpendicular to the *z*-axis is given by the step-size (Fig. 1) of the image stack in the *z*-direction (~0.6 μm for CLSM, ~0.18 μm for SIM), hence the visible gaps in the figures. This distance increases when the track is more slanted (Eq. (5)). The decrease in fluorescence intensity at the end of the measured tracks indicates that alpha particles come to halt within the measured tracks. The point where the alpha particle came to a halt can therefore be estimated using Eq. (6).

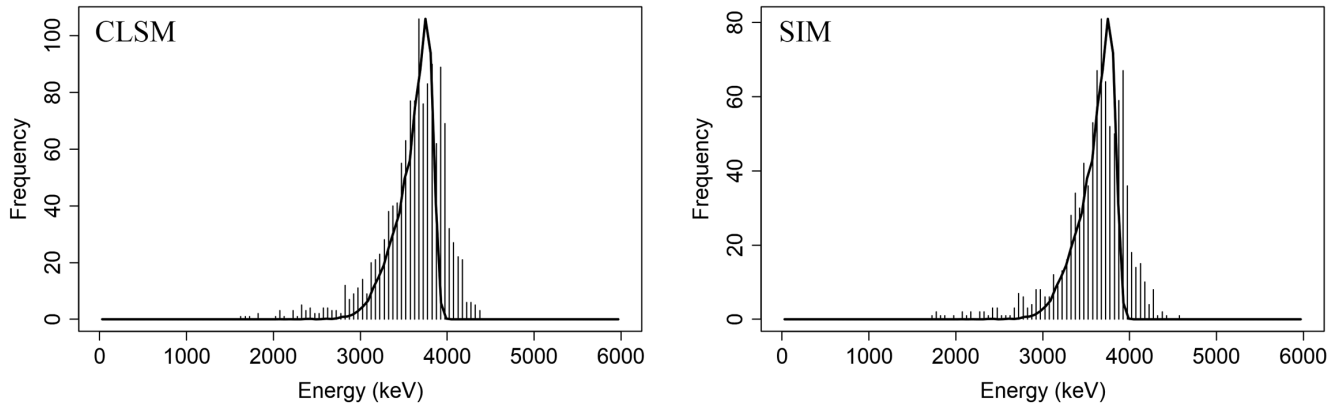

Fig. 4. The energy distribution of alpha particles upon entering the FNTDs for CLSM (left) and SIM (right), calculated using the lengths of the tracks within the FNTD using the described methods. The black line indicates the expected energy distribution obtained from simulations of the experimental setup using the FLUKA software. Peak values for CLSM and SIM were respectively 3682 and 3678 keV.

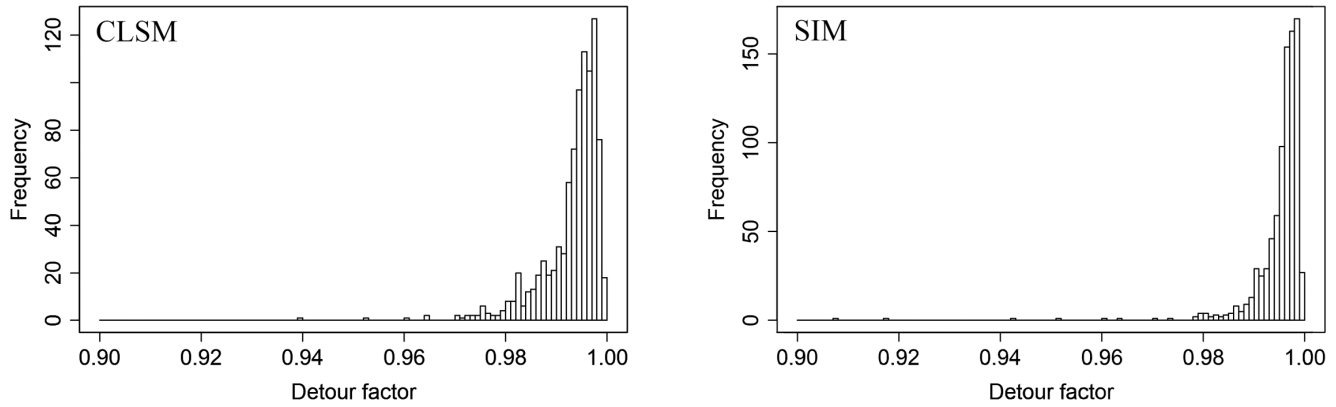

Fig. 5. The detour factor distribution of alpha particles penetrating a FNTD as measured using CLSM (left) and SIM (right). A detour factor of 1 indicates that the particle followed a perfectly straight track through the FNTD, whereas a value close to zero indicates a large deviation from its initial trajectory upon entering the FNTD. The median values for CLSM and SIM were respectively 0.995 and 0.997.

is seen at the end of the tracks for both methodologies, but is more evident with SIM. This allowed for the intensity endpoint fitting approach given in Eq. (6).

Distributions of the calculated alpha particles energies after endpoint refinement are given in Figure 4, together with the distribution obtained from FLUKA simulations. Both the distributions from CLSM and SIM match closely with the expected energy distributions, yielding standard deviations of respectively 306 and 284 keV, compared to 208 keV in the simulation. The exact uncertainty of this method due to noise and resolution for alpha particle energy measurement is unknown, because the true energy distribution is unknown. Although the FLUKA simulation serves as an indicator for the true distribution, this simulation does not account for manufacturing errors in the collimator and degradation of the source. The true energy distribution can therefore reasonably be expected to be broader than the simulation is showing. Nevertheless, for both imaging modalities the proposed method showed a better energy resolution than would likely be achievable using track width or track intensity based methods for alpha radiation (Sykora *et al.*, 2008; Klimpki *et al.*, 2016). It is however important to note that the method proposed in this work is only applicable for tracks ending within the FNTD, which is only the case for (very) low-energy ions, whereas the other methods can be used for all types of tracks.

The detour factor and relative scattering distributions are given in respectively Figures 5 and 6. Given a mean entrance alpha energy of approximately 3900 keV in the FNTD, NIST reports a detour factor in Al_2O_3 of 0.984 (Berger *et al.*, 2005). The mean detour factors for CLSM and SIM were respectively 0.993 and 0.995. As shown in Figures 5 and 6, SIM showed an almost 50% reduction in measured scattering compared to CLSM for the same experiment conditions (Fig. 6), which was most likely the result of the improved resolution of the SIM images, enabling more accurate track reconstruction. These results might be an indication that the simulation approach

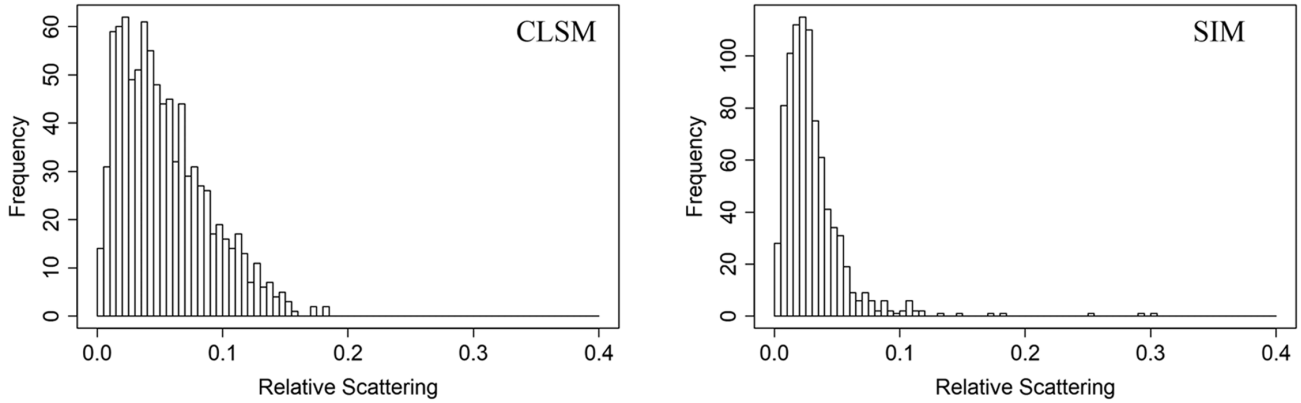

Fig. 6. The relative scattering distribution of alpha particles penetrating a FNTD as measured using CLSM (left) and SIM (right). A relative scattering of 0 indicates a perfectly straight track. The median values for CLSM and SIM were respectively 0.047 and 0.025. Both CLSM and SIM samples were irradiated under the same experimental conditions, indicating that the resolution of CLSM is insufficient to properly measure the scattering of alpha particles.

(Lewis, 1950) used by NIST to estimate the spatial scattering of alpha particles overestimates said scattering of alpha particles in Al_2O_3. Although uncertainty evaluation of particle ranges and scattering is difficult at these low energies, stopping power uncertainties up to 10% for 100 keV alpha particles were reported (ICRU, 1993). Further research is however required to thoroughly estimate the uncertainty in scattering estimation using FNTDs before any concrete conclusions regarding the accuracy of the scattering simulations can be made. Although these results on itself are not expected to make an impact, the overestimation suggests that this method might find its use in Monte Carlo and cross-section validation for low energy ions, a domain that is difficult to validate. Validation of scattering and stopping power data for low-energy alpha particles is important for accurate microdosimetry in alpha radionuclide therapy, a field that studies the effects of alpha radiation on a small (sub-)micron scale and thereby mainly depends on simulation data (Roeske & Stinchcomb, 1997; Kvinnsland *et al.*, 2001; Chouin *et al.*, 2007). The low C and Mg dopant concentrations are expected to be too low to influence the scattering significantly. Figure 7 displays tracks with weak and strong scattering to illustrate that the calculated scattering could be verified via visual inspection.

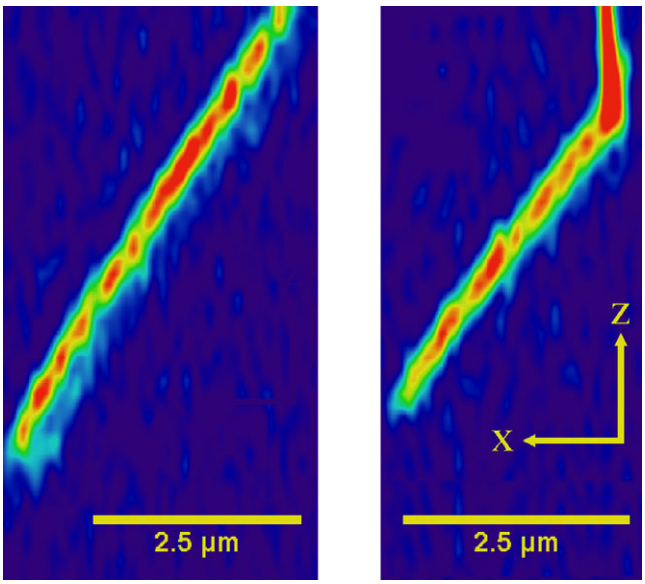

Fig. 7. Alpha particles entering the FNTD, measured using SIM, undergoing no scattering (left) and strong scattering (right). In the absence of heavy collisions between alpha particles and atoms within the FNTD, the alpha particle follows a (close to) perfectly straight path (left). A strong collision with an atom will force to the alpha particle to be deviated from its original path (right). The images of the tracks are maximum intensity projections along the y-axis after alignment of tracks with the x-axis. The relative scattering of the tracks in the left and right were respectively 0.004 and 0.29. Note the change in track intensity when the track angle changes in the right figure due to the change in illumination by the anisotropic excitation beam/spot.

Conclusions and discussion

We have shown for the first time that SIM can be used for quantitative FNTD imaging. The maximum spatial resolution was almost doubled without increasing the scan time. The scan time for SIM could be further reduced by using three instead of five rotations of the illumination pattern, however this would lower the resolution of the reconstructed image and in addition, could lead to an increase of resolution anisotropy. Currently, SIM methods are being developed using different illumination patterns, which require fewer rotations, or no rotations (Chakrova *et al.*, 2015; Schropp *et al.*, 2017) at all and this would further reduce the scan time. Although SIM image reconstruction was computationally intensive and typically took the same amount of time as the image acquisition, the prospect of Graphics Processing Unit (GPU)-based image reconstruction (Lu-Walther *et al.*, 2015; Müller *et al.*, 2017)

is expected to make real-time reconstruction possible in the near future. The proposed method for particle energy estimation based on track length showed an excellent energy resolution, which is required for proper alpha dosimetry. No significant improvement in energy resolution with SIM could be observed compared to CLSM. A significant difference was however visible in the relative spatial scattering of alpha track measurements between the two modalities. The difference in detour factor obtained using SIM versus the numbers obtained from NIST could be an indication that the current data from NIST might be overestimating the scattering of alpha particles in Al_2O_3 and that revision of the current cross section (a measure for interaction probability) might be necessary, but thorough determination of the uncertainty in scattering estimation using FNTDs is required before concrete conclusions can be made regarding the current NIST data. From these results, it is expected that the high resolution of SIM allows for more complex analyses of particle interactions, which can be of great value of the validation of the Monte Carlo simulation code and interaction cross section data. Because ion radiation therapy depends heavily on the accuracy of these simulation codes, the combination of SIM and FNTD imaging might find more applications in this field. Stimulated Emission Depletion (STED) was the only other super-resolution technique applied for FNTDs, but has yet to find its way to wider applications in part due to the long scanning time and technical hardships (Greilich *et al.*, 2013; Niklas *et al.*, 2017). SIM overcomes these challenges by offering super-resolution imaging at scanning speeds compatible with large-scale commercial read-out. The increased resolution can also be used for better detection of secondary particles in clinical carbon beams. Due to the low fluorescence intensity and often large angle of incidence of these secondary particles, their numbers are often underestimated when using CLSM for FNTD read-out (Klimpki *et al.*, 2016). SIM is therefore considered an excellent competitor for high-resolution FNTD read-out, especially with the possibility of fast image acquisition and real-time SIM reconstruction in combination with automatic surface plane detection (Akselrod *et al.*, 2014). The FNTD/SIM combination paves the way for a new type of alpha dosimeter, both for research and personal dosimetry.

Acknowledgements

The authors are grateful to Dr. Mark Akselrod and Landauer Inc. for kindly donating the FNTDs and to STW for funding (project number 13577). This work was facilitated through the Euro-BioImaging Research infrastructure for imaging technologies in biological and biomedical sciences.

References

Akselrod, G.M., Akselrod, M.S., Benton, E.R. & Yasuda, N. (2006) A novel Al2O3 fluorescent nuclear track detector for heavy charged particles and neutrons. *Nucl. Instr. Meth. B* **247**(2), 295–306.

Akselrod, M.S., Akselrod, A.E., Orlov, S.S., Sanyal, S. & Underwood, T.H. (2003) Fluorescent aluminum oxide crystals for volumetric optical data storage and imaging applications. *J. Fluoresc.* **13**, 503–511.

Akselrod, M.S., Fomenko, V.V., Bartz, J.A. & Haslett, T.L. (2014) Automatic neutron dosimetry system based on fluorescent nuclear track detector technology. *Rad. Protect. Dosimetr.* **161**(1), 86–91.

Akselrod, M.S., Yoder, R.C. & Akselrod, G.M. (2006) Confocal fluorescent imaging of tracks from heavy charged particles utilising new Al2O3:C,Mg crystals. *Rad. Protect. Dosimetr.* **119**(1–4), 357–362.

Ball, G., Demmerle, J., Kaufmann, R., Davis, I., Dobbie, I.M. & Schermelleh, L. (2015) SIMcheck: a toolbox for successful super-resolution structured illumination microscopy. *Sci. Rep.* **5**(1), 15915. http://doi.org/10.1038/srep15915

Bandekar, A., Zhu, C., Jindal, R., Bruchertseifer, F., Morgenstern, A. & Sofou, S. (2014) Anti-prostate-specific membrane antigen liposomes loaded with 225Ac for potential targeted antivascular alpha-particle therapy of cancer. *J. Nucl. Med.* **55**(1), 107–114.

Barendsen, G.W., Koot, C.J., Van Kersen, G.R., Bewley, D.K., Field, S.B. & Parnell, C.J. (1966) The effect of oxygen on impairment of the proliferative capacity of human cells in culture by ionizing radiations of different LET. *Int. J. Rad. Biol. Related Stud. Phys., Chem., Med.* **10**(4), 317–327.

Bartz, J.A., Zeissler, C.J., Fomenko, V.V. & Akselrod, M.S. (2013). An imaging spectrometer based on high resolution microscopy of fluorescent aluminum oxide crystal detectors. *Rad. Measure.* **56**, 273–276.

Berger, M.J., Coursey, J.S., Zucker, M.A. & Chang, J. (2005) *ESTAR, PSTAR, and ASTAR: Computer Programs for Calculating Stopping-Power and Range Tables for Electrons, Protons, and Helium Ions (version 1.2.3)*. National Institute of Standards and Technology, Gaithersburg, MD, USA.

Chakrova, N., Heintzmann, R., Rieger, B. & Stallinga, S. (2015) Studying different illumination patterns for resolution improvement in fluorescence microscopy. *Opt. Expr.* **23**(24), 31367. http://doi.org/10.1364/OE.23.031367

Chouin, N., Bitar, A., Lisbona, A., Chérel, M., Davodeau, F., Barbet, J. & Bardiès, M. (2007) Implementation of a microdosimetric model for radioimmunotherapeutic alpha emitters. *Cancer Biother. Radiopharma.* **22**(3), 387–392.

Cucinotta, F.A., Katz, R. & Wilson, J.W. (1998) Radial distribution of electron spectra from high-energy ions. *Rad. Environ. Biophys.* **37**(4), 259–265.

Elgqvist, J., Frost, S., Pouget, J.P. & Albertsson, P. (2014) The potential and hurdles of targeted alpha therapy – clinical trials and beyond. *Front. Oncol.* **3**(January), 1–9.

Ferrari, A., Sala, P.R. & Ranft, J. (2011) *Fluka: A Multi-Particle Transport Code*. Stanford Linear Accelerator Center, Stanford, CA, USA.

Franken, N.A., ten Cate, R., Krawczyk, P.M., Stap, J., Haveman, J., Aten, J. & Barendsen, G.W. (2011) Comparison of RBE values of high-LET α-particles for the induction of DNA-DSBs, chromosome aberrations and cell reproductive death. *Rad. Oncol.* **6**(1), 64. http://doi.org/10.1186/1748-717X-6-64

Greilich, S., Osinga, J.M., Niklas, M. *et al.* (2013) Fluorescent nuclear track detectors as a tool for ion-beam therapy research. *Rad. Measure.* **56**, 267–272.

Gustafsson, M.G.L., Shao, L., Carlton, P.M., Wang, C.J.R., Golubovskaya, I.N., Cande, W.Z., Agard, D.A., Sedat, J.W. (2008) Three-dimensional resolution doubling in wide-field fluorescence microscopy by structured illumination. *Biophys. J.* **94**(12), 4957–4970.

ICRU. (1993) *ICRU Report 49, Stopping Powers and Ranges for Protons and Alpha Particles*.

Jadvar, H. & Quinn, D.I. (2013) Targeted α-particle therapy of bone metastases in prostate cancer. *Clin. Nucl. Med.* **38**(12), 966–971.

Klimpki, G.M., Mescher, H. & Akselrod, M.S. (2016) Fluence-based dosimetry of proton and heavier ion beams using single track detectors. *Phys. Med. Biol.* **61**(3), 1021–1040.

Kouwenberg, J.J.M., Ulrich, L., Jäkel, O. & Greilich, S. (2016) A 3D feature point tracking method for ion radiation. *Phys. Med. Biol.* **61**(11), 4088–4104.

Kvinnsland, Y., Stokke, T. & Aurlien, E. (2001) Radioimmunotherapy with alpha-particle emitters: microdosimetry of cells with a heterogeneous antigen expression and with various diameters of cells and nuclei. *Rad. Res.* **155**(2), 288–296.

Lewis, H.W. (1950) Multiple scattering in an infinite medium. *Phys. Rev.* **78**(5), 526–529.

Lu-Walther, H.-W., Kielhorn, M., Förster, R., Jost, A., Wicker, K. & Heintzmann, R. (2015) fastSIM: a practical implementation of fast structured illumination microscopy. *Meth. Appl. Fluor.* **3**(1), 14001. http://doi.org/10.1088/2050-6120/3/1/014001

Lukosz, W. & Marchand, M. (1963) Optischen Abbildung Unter Überschreitung der Beugungsbedingten Auflösungsgrenze. *Optica Acta: Int. J. Opt.* **10**(3), 241–255.

Müller, M., Markwirth, A., Mönkemöller, V., Lachetta, M., Wilking, A., Hübner, W. & Huser, T. (2017) *Video-Rate, Multi-Color Structured Illumination Microscopy with GPU-Based, Immediate Image Reconstruction, Biomolecular Photonics*. Bielefeld University, Bielefeld, Germany.

Niklas, M., Henrich, M., Jäkel, O., Engelhardt, J., Abdollahi, A. & Greilich, S. (2017) STED microscopy visualizes energy deposition of single ions in a solid-state detector beyond diffraction limit. *Phys. Med. Biol.* **62**(9), N180–N190.

R Core Development Team. (2011) *R: A Language and Environment for Statistical Computing, R Foundation for Statistical Computing*. The R Foundation for Statistical Computing, Vienna, Austria. Vienna, Austria.

Roeske, J.C. & Stinchcomb, T.G. (1997) Dosimetric framework for therapeutic alpha-particle emitters. *J. Nucl. Med.* **38**, 1923–1929.

Sartor, O., Maalouf, B.N., Hauck, C.R. & Macklis, R.M. (2012) Targeted use of alpha particles: current status in cancer therapeutics. *J. Nucl. Med. Rad. Ther.* **3**(4). http://doi.org/10.4172/2155-9619.1000136

Schindelin, J., Rueden, C.T., Hiner, M.C. & Eliceiri, K.W. (2015) The ImageJ ecosystem: an open platform for biomedical image analysis. *Mol. Reprod. Dev.* **82**(7), 518–529.

Scholz, M. & Kraft, G. (1996) Track structure and the calculation of biological effects of heavy charged particles. *Adv. Space Res.* **18**(1–2), 5–14.

Schropp, M., Seebacher, C. & Uhl, R. (2017). XL-SIM: extending superresolution into deeper layers. *Photonics* **4**(2), 33. http://doi.org/10.3390/photonics4020033

Sgouros, G., Roeske, J.C., McDevitt, M.R. *et al.* (2010) MIRD Pamphlet No. 22 (abridged): radiobiology and dosimetry of alpha-particle emitters for targeted radionuclide therapy. *J. Nucl. Med.* **51**(2), 311–328.

Sofou, S., Thomas, J.L., Lin, H., McDevitt, M.R., Scheinberg, D.A. & Sgouros, G. (2004) Engineered liposomes for potential alpha-particle therapy of metastatic cancer. *J. Nucl. Med.* **45**(2), 253–260.

Sykora, G.J., Akselrod, M.S., Benton, E.R. & Yasuda, N. (2008) Spectroscopic properties of novel fluorescent nuclear track detectors for high and low LET charged particles. *Rad. Measure.* **43**, 422–426.

Sykora, G.J., Akselrod, M.S. & Vanhavere, F. (2009) Performance of fluorescence nuclear track detectors in mono-energetic and broad spectrum neutron fields. *Rad. Measure.* **44**(9–10), 988–991.

Tracy, B.L., Stevens, D.L., Goodhead, D.T. & Hill, M.A. (2015) Variation in RBE for survival of V79-4 cells as a function of alpha-particle (helium ion) energy. *Rad. Res.* **184**(1), 33–45.

Van Elburg, H.J., Kuypers, L.C., Decraemer, W.F. & Dirckx, J.J.J. (2007) Improved correction of axial geometrical distortion in index-mismatched fluorescent confocal microscopic images using high-aperture objective lenses. *J. Microsc.* **228**(1), 45–54.

Supporting Information

Additional Supporting information may be found in the online version of this article at the publisher's website:

Fig. S1. Full field of view of FNTD irradiated with alpha radiation and imaged with CLSM and SIM. (A) Single image from the middle of a CLSM 3D-stack. (B) Max projection of the same 3D image stack. (C) Single image from the middle of a SIM 3D-stack. (D) Maximum projection of the same 3D image stack. The yellow boxes indicate the field of view shown in Fig. 2. The CLSM images were cropped to match the field of view of the SIM data (75 μm × 75 μm). Scale bars are 10 micrometre.

Fig. S2. FNTD orientation-dependent shadow tracks. Maximum projections of SIM images obtained at the indicated FNTD sample orientation. Shadow tracks are indicated by arrows. CLSM image is shown for comparison. Scale bar is 2 μm. Graph displays the average line plot across a single track (red line) for FNTD at 260° (indicated by *). The blue and black lines are the average line plots for tracks imaged by CLSM and SIM (FNTD at 0°), respectively. The resolution of CLSM is too low to detect shadow tracks.

Fig. S3. SIM check was performed on both raw and reconstructed data. (A) Cropped area of raw and reconstructed data. The full image was used for SIMcheck. (B) modulation contrast to noise ratio (MCNR) of raw and reconstructed data. MCNR is depicted on a colour scale, where orange to yellow pixels indicate moderate to good modulation. (C) Channels intensity profile of raw data, the total intensity variation measured is 30.5%. (D) Fourier transform analysis of reconstructed data of both a lateral (*xy*) and a radial view, no clear artefacts were observed. (E) Spherical aberration mismatch analysis minimum values (black line) and maximum values (grey line) are depicted a *z*-minimum variation of 0.0523 was measured. (F) Reconstructed intensity profile on a linear (black) and a logarithmic (grey) scale, a min-to-max intensity ratio of 3.30 was measured.